frontiers | Frontiers in Plant Science

TYPE Original Research
PUBLISHED 06 March 2025
DOI 10.3389/fpls.2025.1478346

OPEN ACCESS

EDITED BY
Weimin Ma,
Shanghai Normal University, China

REVIEWED BY
Jun Li,
Chinese Academy of Sciences (CAS), China
Jianqiang He,
Northwest A & F University, China

*CORRESPONDENCE
Shuang-Xi Zhou
shuangxi.zhou@dpird.wa.gov.au
Zi-Piao Ye
yezp@jgsu.edu.cn

†These authors have contributed equally to this work

RECEIVED 09 August 2024
ACCEPTED 04 February 2025
PUBLISHED 06 March 2025

CITATION
Yang X-L, An T, Ye Z-W-Y, Kang H-J, Robakowski P, Ye Z-P, Wang F-B and Zhou S-X (2025) Modeling light response of effective quantum efficiency of photosystem II for C_3 and C_4 crops.
Front. Plant Sci. 16:1478346.
doi: 10.3389/fpls.2025.1478346

Modeling light response of effective quantum efficiency of photosystem II for C_3 and C_4 crops

Xiao-Long Yang[1,2†], Ting An[3†], Zi-Wu-Yin Ye[4], Hua-Jing Kang[5], Piotr Robakowski[6], Zi-Piao Ye[7,8*], Fu-Biao Wang[8] and Shuang-Xi Zhou[9*]

[1]School of Life Sciences, Nantong University, Nantong, China, [2]State Key Laboratory of Environmental Chemistry and Ecotoxicology, Research Center for Eco-Environmental Sciences, Chinese Academy of Sciences, Beijing, China, [3]College of Bioscience and Bioengineering, Jiangxi Agricultural University, Nanchang, China, [4]School of Foreign Languages, Guangdong Baiyun University, Guangzhou, China, [5]Key Laboratory of Crop Breeding in South Zhejiang, Wenzhou Academy of Agricultural Sciences, Wenzhou, China, [6]Department of Forestry and Wood Technology, Poznan University of Life Sciences, Poznan, Poland, [7]New Quality Productivity Research Center, Guangdong ATV College of Performing Arts, Deqing, China, [8]Math & Physics College, Jinggangshan University, Ji'an, China, [9]Department of Biological Sciences, Macquarie University, Sydney, NSW, Australia

Effective quantum efficiency of photosystem II (Φ_{PSII}) represents the proportion of photons of incident light that are actually used for photochemical processes, which is a key determinant of crop photosynthetic efficiency and productivity. A robust model that can accurately reproduce the nonlinear light response of Φ_{PSII} (Φ_{PSII}–*I*) over the I range from zero to high irradiance levels is lacking. In this study, we tested a Φ_{PSII}–*I* model based on the fundamental properties of light absorption and transfer of energy to the reaction centers via photosynthetic pigment molecules. Using a modeling-observation intercomparison approach, the performance of our model versus three widely used empirical Φ_{PSII}–*I* models were compared against observations for two C_3 crops (peanut and cotton) and two cultivars of a C_4 crop (sweet sorghum). The results highlighted the significance of our model in (1) its accurate and simultaneous reproduction of light response of both Φ_{PSII} and the photosynthetic electron transport rate (*ETR*) over a wide I range from light limited to photoinhibition *I* levels and (2) accurately returning key parameters defining the light response curves.

KEYWORDS

Ye model, effective quantum efficiency of photosystem II (Φ_{PSII}), non-photochemical quenching, light absorption cross-section, light-harvesting pigment molecules, photosynthetic light response

Introduction

Light intensity (*I*; see Table 1 for list of abbreviations and definitions) exhibits dynamic fluctuations across various temporal scales, ranging from seconds to months due to wind-induced leaf movements and diurnal solar variations (Liu et al., 2021). Under low *I* conditions, plants efficiently channel the majority of absorbed light to reaction centers for photochemical processes. Under high *I* conditions, plants dissipate approximately 80% of absorbed light as heat through non-photochemical quenching (*NPQ*) to prevent light damage (Niyogi and Truong, 2013). The generation of *NPQ* primarily originates from the de-excitation of light-harvesting pigment molecules in excited state (N_k). Consequently, there exists a significant correlation between the quantity of N_k and the magnitude of *NPQ*. Additionally, the light environment within leaves is highly heterogeneous due to the focusing effect of epidermal cells and the light-guiding properties of vascular bundle sheath structures (Xiao et al., 2016; Song et al., 2017). This heterogeneity results in significant *I* variations among different cells within the leaf and even among chloroplasts within the same mesophyll cell (Xiao et al., 2016). Photosystems within chloroplasts constantly operate in a highly dynamic light environment, and accurate modeling of photosynthetic responses to rapid change of *I* is important for us to understand the adaptive responses of plants to the changing light environments.

Photosystem II (PSII) is pivotal in the light-dependent reactions of photosynthesis, driving the initial steps of energy conversion. Its activity can be conveniently assayed using bio-optical techniques (Buckley and Farquhar, 2004; Robakowski, 2005; Baker, 2008; Pavlovič et al., 2011; Shevela et al., 2023), with chlorophyll *a* fluorescence being the most widely adopted method. This technique facilitates the research into several key photosynthetic properties, including the maximum quantum efficiency of PSII (F_v/F_m), the effective quantum efficiency of PSII [$\Phi_{PSII} = (F_m' - F')/F_m'$, where F_m' is the maximum fluorescence in the light and F' is steady-state fluorescence], the photosynthetic electron transport rate (*ETR*) and *NPQ*. In addition, given that the generation of *NPQ* mainly results from the de-excitation of N_k, the concurrent change in N_k and *NPQ* with the increasing *I* should be able to be characterized with a robust model.

Φ_{PSII} and *ETR* are the most widely used photochemical parameters to assess the efficiency of plant photochemistry in different environments (Genty et al., 1989; Moin et al., 2016). Φ_{PSII} represents the proportion of photons of incident light that are actually used to drive photochemistry, and it is closely linked with the closure and opening of PSII in photosynthetic primary reactions and chlorophyll fluorescence emission (Baker, 2008). Meanwhile, *ETR* is closely related to Φ_{PSII} and *I* (Genty et al., 1989; Krall and Edwards, 1992). Many studies using fluorescence techniques to determine Φ_{PSII} found it decreasing nonlinearly with the increasing *I* (Robakowski, 2005; Pavlovič et al., 2011; van der Tol et al., 2014; Córdoba et al., 2016). With the increasing *I*, *ETR* initially increased, and then, it reached a platform or there occurred photoinhibition or dynamic downregulation of PSII at high light intensities. This nonlinear relationship reflects the complex interplay between light absorption, energy transfer, and dissipation mechanisms in the photosynthetic apparatus, highlighting the adaptive responses of plants to varying environments.

No model has yet been reported to simultaneously accurately reproduce Φ_{PSII}–*I* and *ETR*–*I* curves over a wide I range from zero to photoinhibitory *I* levels. Among the limited studies characterizing the Φ_{PSII}–*I* curve, the negative exponential function and the exponential function are the most widely used models (Webb et al., 1974; Smyth et al., 2004; Ritchie, 2008; Ritchie and Bunthawin, 2010; Silsbe and Kromkamp, 2012; Robakowski et al., 2018). However, it has been reported that the values of I_{sat} estimated by the negative exponential functions are significantly higher than the measured values (Robakowski, 2005; Ritchie, 2008; Ritchie and Bunthawin, 2010). In addition, the non-rectangular hyperbolic model (NRH model) is the most widely used to characterize the *ETR*–*I* curve and returning ETR_{max} (von Caemmerer, 2000; Long and Bernacchi, 2003; Miao et al., 2009; Yin et al., 2009; Gu et al., 2010; Bernacchi et al., 2013; von Caemmerer, 2013; Buckley and Diaz-Espejo, 2015; Cai et al., 2018; Yin et al., 2021). However, the NRH model significantly have been reported to overestimate ETR_{max}, and it cannot return a realistic I_{sat} due to its asymptotic function (Buckley and Diaz-Espejo, 2015; Yang et al., 2024). Experimentally, the value of $\Phi_{PSIImax}$ was measured when *I* was 0 μmol photons m^{-2} s^{-1}.

In this study, we aimed to develop and test a Φ_{PSII}–*I* model based on the fundamental properties of light absorption of photosynthetic pigment molecules (Ye et al., 2013a, 2013b). We evaluated the performance of the model using a modeling-observation intercomparison approach against observations conducted on two C_3 corps (peanut and cotton) and two genotypes of a C_4 crop (sweet sorghum cultivars KFJT-1 and KFJT-4). We also compared the robustness of this model against three widely used empirical *ETR*–*I* and Φ_{PSII}–*I* models (i.e., the negative exponential function, the exponential function, and the NRH model) in their performances of (1) reproducing the observed light response curves and (2) returning key parameters defining the curves (i.e., $\Phi_{PSIImax}$, ETR_{max} and the corresponding I_{sat}).

Materials and methods

Plant materials

Seeds of peanut (*Arachis hypogaea* L.) and cotton (*Gossypium hirsutum* L.) were surface disinfected with 70% ethanol and 20% bleach, then planted in trays and placed in an RDN-1000E-4 growth chamber (Ningbo Dongnan Instrument Co., China) under conditions of 23°C and 28°C (16 h/8 h light/dark cycle) for cultivation. When the seedlings developed two cotyledons, they were transplanted into the fields of the Botanical Garden at Nantong University. Field management was carried out according to the previously described methods (Wang et al., 2017). Seedling cultivation of sweet sorghum (*Sorghum bicolor* L. Moench, KFJT-1 and KFJT-4) followed the

10.3389/fpls.2025.1478346

TABLE 1 List of major model parameters defining the light response curves of effective quantum efficiency of photosystem II (Φ_{PSII}) and electron transport rate (*ETR*).

Symbol	Definition	Unit
ETR	Electron transport rate	μmol electrons m^{-2} s^{-1}
ETR_{max}	Maximum electron transport rate	μmol electrons m^{-2} s^{-1}
F	Steady-state fluorescence	
F_m	Maximum fluorescence in the dark adaptation	
F_m'	Maximum fluorescence in the light	
F_v	Variable fluorescence yield of the dark-adapted leaf PSII	
F_v/F_m	Maximum quantum efficiency of PSII	
g_i	Degeneration of energy level of photosynthetic pigment molecules in the ground state *i*	
g_k	Degeneration of energy level of photosynthetic pigment molecules in the excited state *k*	
I	Photon flux densities or light intensity	μmol photons m^{-2} s^{-1}
k_P	Rate of photochemical reaction	s^{-1}
k_D	Rate of heat loss	s^{-1}
α_e	Initial slope of the light response curve of electron transport rate	μmol electrons (μmol photons)$^{-1}$
β_e	Dynamic down-regulation term of PSII	m^2 s (μmol photons)$^{-1}$
γ_e	Saturation term of photosynthesis	m^2 s (μmol photons)$^{-1}$
NPQ	Non-photochemical quenching	
a	Initial slope of the light response curve of non-photochemical quenching	
b	*b* is equivalent to γ_e, the saturation term of photosynthesis	
NPQ_0	Total light-harvesting pigment molecules	
N_k	Total light-harvesting pigment molecules in excited state *k*	
I_{sat}	Saturation light intensity corresponding to ETR_{max}	μmol photons m^{-2} s^{-1}
ξ_1	Probability of photochemistry	
ξ_2	Probability of heat loss	
ξ_3	Probability of fluorescence	
R_{ki}	Relaxation rate by spontaneous emission from excited state *k* to ground state *i*	s^{-1}
σ_{ik}	Eigen-absorption cross-section of photosynthetic pigment from ground state *i* to excited state *k* due to light illumination	m^2
σ_{ik}	Effective absorption cross-section of light-harvesting pigment molecules	m^2
φ	Exciton-use efficiency in PSII	
τ	Average lifetime of the photosynthetic pigment molecules in the lowest excited state	s
Φ_{PSII}	Effective quantum efficiency of PSII	
$\Phi_{PSIImax}$	Maximum effective quantum efficiency of PSII	

(Continued)

protocols established in our previous research (Yang et al., 2024). These two strains were developed by the Institute of Modern Physics, Chinese Academy of Sciences, through heavy ion irradiation of the parental line KFJT-CK. The cultivated seedlings were transferred to plastic pots and placed in a climate-controlled chamber, where they were grown under 25,000 lx light intensity, at 25°C, and with a 16 h/8 h light/dark cycle. Healthy plants bearing eight leaves were selected for data measurements for each species.

Analytical models

Model 1 (Ye model)

The Ye model provides a mechanistic framework for describing the light response of *ETR* in PSII based on the biophysical properties of light-harvesting pigment molecules using Equation 1 (Ye et al., 2013a, 2013b):

$$ETR = \frac{\alpha\beta N_0 \sigma_{ik} \varphi}{S} \times \frac{1 - \frac{\left(1-\frac{g_i}{g_k}\right)\sigma_{ik}\tau}{\xi_3+(\xi_1 k_P+\xi_2 k_D)\tau} I}{1 + \frac{\left(1-\frac{g_i}{g_k}\right)\sigma_{ik}\tau}{\xi_3+(\xi_1 k_P+\xi_2 k_D)\tau} I} I \quad (1)$$

where φ is the exciton-use efficiency in PSII, N_0 is total photosynthetic pigment molecules of the measured leaf, *S* is the leaf area (m^2), and g_i and g_k are the degeneration of energy levels of photosynthetic pigments in the ground state (*i*) and excited state (*k*), respectively. k_P and k_D are rates of the photochemical reaction and heat loss, respectively (Baker, 2008). ξ_1, ξ_2, and ξ_3 are the occupation probability of photochemistry, heat loss, and fluorescence emission, respectively. σ_{ik} is the eigen-absorption cross-section of photosynthetic pigments from the ground state *i* to the excited state *k* via light exposure, and τ is the average lifetime of the photosynthetic pigments in the lowest excited state *k*.

To simplify Equation 1, three aggregate parameters encapsulating biophysical dynamics are introduced: $\alpha_e = \frac{\alpha\beta N_0 \sigma_{ik} \varphi}{S}$ [μmol electrons (μmol photons)$^{-1}$] represents the initial slope of the light response curve of electron transport rate (*ETR*–*I* curve), $\beta_e = \frac{\left(1-\frac{g_i}{g_k}\right)\sigma_{ik}\tau}{\xi_3+(\xi_1 k_P+\xi_2 k_D)\tau}$ [m^2 s (μmol photons)$^{-1}$] reflects the dynamic downregulation term of PSII, and $\gamma_e = \frac{\left(1+\frac{g_i}{g_k}\right)\sigma_{ik}\tau}{\xi_3+(\xi_1 k_P+\xi_2 k_D)\tau}$ [m^2 s (μmol photons)$^{-1}$] represents the saturation term of photosynthesis.

With these parameters, Equation 1 simplifies to:

$$ETR = \alpha_e \frac{1-\beta_e I}{1+\gamma_e I} I \quad (2)$$

Equations 1 and 2 describe *ETR*–*I* function and depict the interdependence between *ETR* and biophysical parameters.

Since Equation 1 is a non-asymptotic function, it has the first derivative. When the first derivative of Equation 1 equals to zero, I_{sat} is calculated as follows:

$$I_{sat} = \frac{\sqrt{\frac{(\beta_e+\gamma_e)}{\beta_e}}-1}{\gamma_e} \quad (3)$$

Substituting Equation 3 into Equation 2, the maximum *ETR* (ETR_{max}) can be determined using Equation 4:

$$ETR_{max} = \alpha_e \left(\frac{\sqrt{\beta_e+\gamma_e}-\sqrt{\beta_e}}{\gamma_e} \right)^2 \quad (4)$$

Moreover, combing Equation 1 with $ETR = \alpha \times \beta \times \Phi_{PSII} \times I$ (Krall and Edwards, 1992), the relationship between Φ_{PSII} and *I* can be described as follows:

$$\Phi_{PSII} = \frac{N_0 \sigma_{ik} \varphi}{S} \times \frac{1-\frac{\left(1-\frac{g_i}{g_k}\right)\sigma_{ik}\tau}{\xi_3+(\xi_1 k_P+\xi_2 k_D)\tau} I}{1+\frac{\left(1-\frac{g_i}{g_k}\right)\sigma_{ik}\tau}{\xi_3+(\xi_1 k_P+\xi_2 k_D)\tau} I} I \quad (5)$$

Simplified, this becomes:

$$\Phi_{PSII} = \Phi_{PSIImax} \frac{1-\beta_e I}{1+\gamma_e I} \quad (6)$$

where $\Phi_{PSIImax} = \frac{\alpha_e}{\alpha\beta}$.

The effective absorption cross-section of light-harvesting pigment molecules (σ'_{ik}), which represents its ability to absorb light energy with *I*, can also be expressed as a function of *I* (Ye et al., 2013b). Namely,

$$\sigma'_{ik} = \frac{\sigma_{ik}}{1+\frac{\left(1-\frac{g_i}{g_k}\right)\sigma_{ik}\tau I}{\xi_3+(\xi_1 k_P+\xi_2 k_D)\tau}} \times \left[1-\frac{\left(1-\frac{g_i}{g_k}\right)\sigma_{ik}\tau I}{\xi_3+(\xi_1 k_P+\xi_2 k_D)\tau} \right] \quad (7)$$

Equation 7 shows that σ'_{ik} increases with k_P, k_D, ξ_1, ξ_2, ξ_3, and $1/\tau$ but decreases with *I*. $\sigma'_{ik} = \sigma_{ik}$ when $I = 0$ μmol photons m^{-2} s^{-1}. As such, the light absorption cross-section is not a constant under any given *I* (excluding $I = 0$ μmol photons m^{-2} s^{-1}). By introducing β_e and γ_e, Equation 7 can be simplified to:

$$\sigma'_{ik} = \frac{1-\beta_e I}{1+\gamma_e I} \sigma_{ik} \quad (8)$$

Comparing Equation 5 with Equation 7, the relationship between Φ_{PSII} and σ'_{ik} is described by Equation 9:

$$\Phi_{PSII} = \Phi_{PSIImax} \frac{\sigma'_{ik}}{\sigma_{ik}} \quad (9)$$

For a given species under given environmental conditions, the values of $\Phi_{PSIImax}$ and σ_{ik} are constants. Equation 9 demonstrates that Φ_{PSII} is directly proportional to σ'_{ik}, and it changes as a function of σ'_{ik}.

The number of photosynthetic pigment molecules in the excited state *k* (N_k) can be expressed as:

$$N_k = \frac{\sigma_{ik}\tau I}{\left(1-\frac{g_i}{g_k}\right)\sigma_{ik}\tau I + (\xi_3+\xi_1 k_P \tau + \xi_2 k_D \tau)} N_0 \quad (10)$$

Equation 10 demonstrates that N_k is a dynamic variable, exhibiting continuous fluctuations rather than maintaining constant values. N_k decreases with k_P, k_D, ξ_1, ξ_2, and ξ_3 but increases with σ_{ik}, τ, and *I*. Under dark conditions ($I = 0$ μmol photons m^{-2} s^{-1}), it must be that N_k equals 0.

By applying β_e and γ_e to Equation 10, it can be simplified to:

$$N_k = \frac{1}{1-\frac{g_i}{g_k}} \times \frac{\beta_e I}{1+\gamma_e I} N_0 \quad (11)$$

Equation 11 shows that N_k increases with the increasing *I*.

Considering that chlorophyll fluorescence primarily stems from light-harvesting pigment molecules in the excited state, it is logical to infer that *NPQ* response to *I* would closely mirror the response of N_k to *I*. Building on Equation 11, the light response expression for *NPQ* can be deduced from the light response model of N_k, the expression for *NPQ* in response to light can be derived as:

$$NPQ = NPQ_{max} \frac{aI}{1+bI} + NPQ_0 \quad (12)$$

where $a = \frac{\beta_e}{1-\frac{g_i}{g_k}}$ is initial slope of the light response curve of *NPQ*, $b = \frac{\left(1-\frac{g_i}{g_k}\right)\sigma_{ik}\tau}{\xi_3+(\xi_1 k_P+\xi_2 k_D)\tau}$ is equivalent to γ_e, the saturation term of photosynthesis, and NPQ_0 is *NPQ* at $I = 0$ μmol photons m^{-2} s^{-1}.

Equations 2, 5 (and 6), 8, 11, and 12 represent how Model 1 (Ye model) describes Φ_{PSII}–*I*, *ETR*–*I*, σ'_{ik}–*I* N_k–*I*, and *NPQ*–*I* curves, respectively.

Model 2 (negative exponential function)

It has been found experimentally that Φ_{PSII}, ranging from 0 to 1, usually follows a simple negative exponential function as follows (Ritchie, 2008; Ritchie and Bunthawin, 2010; Buckley and Diaz-Espejo, 2015):

$$\Phi_{PSII} = \Phi_{PSIImax} \times e^{-k_w I} \quad (13)$$

where $\Phi_{PSIImax}$ is defined as the maximum effective quantum efficiency when $I = 0$ μmol photons m^{-2} s^{-1}, k_w is a scaling constant, and *I* is the light intensity. The values of $\Phi_{PSIImax}$ and k_w can be obtained when Φ_{PSII}–*I* curves are simulated by Equation 13.

Substituting Equation 13 into $ETR = \alpha\times\beta\times\Phi_{PSII}\times I$ (Krall and Edwards, 1992), we get the following expression for *ETR*:

$$ETR = \alpha \times \beta \times I \times \Phi_{PSIImax} \times e^{-k_w I} \quad (14)$$

When the first derivative of Equation 14 equals to zero, we can calculate saturation I (I_{sat}=1/k_w), then substitute k_w =1/I_{sat} into Equation 14 to determine the maximum electron transport rate ($ETR_{max} = \alpha\times\beta\times I_{sat}\times\Phi_{PSIImax}\times e^{-1}$).

Equations 13 and 14 represent how the negative exponential function (Model 2) describes Φ_{PSII}–*I* and *ETR*–*I* curves. It should be noted that there are two values of $\Phi_{PSIImax}$ to be returned when both Φ_{PSII}–*I* and *ETR*–*I* curves are simulated by Equations 13 and 14, respectively.

Model 3 (exponential function)

The exponential function was introduced to simulate Φ_{PSII}–*I* curves as follows (Smyth et al., 2004; Silsbe and Kromkamp, 2012):

$$\Phi_{PSII} = \frac{F_v}{F_m} \times \frac{I_{sat}}{I}\left[1 - \exp\left(-\frac{I}{I_{sat}}\right)\right] \quad (15)$$

where F_v/F_m is the "dark-adapted" maximum operating efficiency of PSII, and I_{sat} is the saturation *I* (Smyth et al., 2004). However, it should be noted that $\Phi_{PSIImax}$ cannot be estimated by Equation 15, but I_{sat} and F_v/F_m can be estimated when Φ_{PSII}–*I* curve is fitted by Equation 15.

Similarly, substituting Equation 15 into $ETR = \alpha\times\beta\times\Phi_{PSII}\times I$ (Krall and Edwards, 1992), we get the following expression for *ETR*:

$$ETR = \alpha \times \beta \times \frac{F_v}{F_m} \times I_{sat}\left[1 - \exp(-\frac{I}{I_{sat}})\right] \quad (16)$$

The values of I_{sat} and F_v/F_m can be returned when *ETR*–*I* curves are simulated by Equation 16.

The maximum *ETR* can be calculated by Equation 17:

$$ETR_{max} = \alpha \times \beta \times \frac{F_v}{F_m} \times I_{sat}[1 - \exp(-1)] \quad (17)$$

Equations 15 and 16 represent how the exponential function (Model 3) describes Φ_{PSII}–*I* and *ETR*–*I* curves. Similarly, it should be noted that there are two values of I_{sat} and F_v/F_m to be returned when both Φ_{PSII}–*I* and *ETR*–*I* curves are simulated by Equations 15 and 16, respectively.

Model 4 (non-rectangular hyperbolic model)

The non-rectangular hyperbolic (NRH) model has been mainly used to fit the *ETR*–*I* curves of plants (von Caemmerer, 2000; Long and Bernacchi, 2003; Miao et al., 2009; Yin et al., 2009; Gu et al., 2010; Bernacchi et al., 2013; von Caemmerer, 2013; Buckley and Diaz-Espejo, 2015; Cai et al., 2018; Yin et al., 2021), and it has been a sub-model in the FvCB model when irradiance is below the saturation level (Farquhar et al., 1980; von Caemmerer, 2000, 2013; Park et al., 2016; Yin et al., 2021). In the NRH model, the dependence of *ETR* on *I* can be expressed as follows:

$$ETR = \frac{\alpha' \times I + ETR_{max} - \sqrt{(\alpha' \times I + ETR_{max})^2 - 4\theta \times \alpha' \times I \times ETR_{max}}}{2\theta} \quad (18)$$

where α' is defined as the initial slope of the *ETR*–*I* curve, θ is a degree of curvature, and ETR_{max} is the maximum *ETR*. Because the first derivative of Equation 18 is always greater than zero, we cannot use Equation 18 to estimate I_{sat}.

Similarly, combing Equation 18 with $ETR = \alpha\times\beta\times\Phi_{PSII}\times I$ (Krall and Edwards, 1992), we get the following expression for Φ_{PSII}:

$$\Phi_{PSII} = \frac{\alpha' \times I + ETR_{max} - \sqrt{(\alpha' \times I + ETR_{max})^2 - 4\theta \times \alpha' \times I \times ETR_{max}}}{2\theta \times \alpha \times \beta \times I} \quad (19)$$

Equations 18 and 19 represent how the NRH model (Model 4) describes *ETR*–*I* and Φ_{PSII}–*I* curves. However, it should be noted that $\Phi_{PSIImax}$ and its corresponding I_{sat} cannot be estimated by Equation 19. In addition, there are two values of ETR_{max} to be returned when both *ETR*–*I* and Φ_{PSII}–*I* curves are simulated by Equations 18 and 19, respectively.

Chlorophyll a fluorescence measurement

Measurements were performed on plant leaves using a LI-6800 portable photosynthesis system (LI-COR Inc., USA) equipped with a LI-6800-01A leaf chamber fluorometer (LI-COR Inc., USA). A fully unfolded, dark green, and healthy leaf was used for each measurement. The initial fluorescence (F_0) was recorded after 25 min of dark adaptation in the cuvette. The maximal fluorescence level of the dark-adapted leaves (F_m) and light-adapted leaves (F_m') were determined by applying saturating flashes (15,000 μmol photons m^{-2} s^{-1}) lasting 1 s, to promote the closure of the PSII reaction centers (Maxwell and Johnson, 2000). F_v/F_m and *NPQ* were calculated as $(F_m–F_0)/F_m$ and $(F_m–F_m')/F_m'$, respectively (van Kooten and Snel, 1990).

Light response measurements were conducted on sunny days from 8:30–11:30 a.m. to 2:00–5:00 p.m. using the automatic measurement program of the LI-6800 system. Leaves were flatly clamped into the leaf chamber and gradually exposed to light intensities of 0 μmol photons m^{-2} s^{-1}, 25 μmol photons m^{-2} s^{-1}, 50 μmol photons m^{-2} s^{-1}, 100 μmol photons m^{-2} s^{-1}, 200 μmol photons m^{-2} s^{-1}, 300 μmol photons m^{-2} s^{-1}, 400 μmol photons m^{-2} s^{-1}, 600 μmol photons m^{-2} s^{-1}, 800 μmol photons m^{-2} s^{-1}, 1,000 μmol photons m^{-2} s^{-1}, 1,200 μmol photons m^{-2} s^{-1}, 1,400 μmol photons m^{-2} s^{-1}, 1,600 μmol photons m^{-2} s^{-1}, 1,800 μmol photons m^{-2} s^{-1}, 1,900 μmol photons m^{-2} s^{-1}, to 2,000 μmol photons m^{-2} s^{-1}. For each light intensity, a minimum waiting time of 2 min and a maximum waiting time of 3 min were set before recording data. The instrument automatically matched the reference and sample chambers before data recording to ensure accuracy. The ambient CO_2 concentration in the leaf chamber was maintained at 410 μmol mol^{-1}, supplied via an external CO_2 gas cylinder connected to the instrument's CO_2 injection system, with a flowrate of 500 μmol s^{-1}. Air temperature in the leaf chamber was set at 30°C. Before measurements, leaves were exposed to sunlight or a light intensity of 1,800 μmol photons m^{-2} s^{-1} for 40 min to ensure activation. *ETR* was calculated as $ETR = \alpha\times\beta\times\Phi_{PSII}\times I$, where α is the distribution coefficient of absorption light energy by PSII and PSI, assumed to be 0.5 (Krall and Edwards, 1992; Maxwell and Johnson, 2000; Evans,

2009), and β is leaf absorptance, assumed to be 0.84 (Ehleringer, 1981). In this study, the values of Φ_{PSII} at I = 0 μmol photons m^{-2} s^{-1} were taken as the maximum Φ_{PSII} ($\Phi_{PSIImax}$). Key parameters (e.g., $\Phi_{PSIImax}$, ETR_{max}, F_v/F_m, and I_{sat}) from *ETR*–*I* curves and Φ_{PSII}–*I* curves were fitted using Model 1–4, respectively, with SPSS 24.0 statistical software (SPSS, Chicago, IL).

Chlorophyll content

Leaf disks were removed from the labeled leaves, followed by rapidly clipping of leaf area of 1 cm diameter for each leaf, to be cut into fine shreds and placed into glass test tube containing 5 mL of 80% (v/v) acetone. The airtight tubes were placed in the dark overnight or until the leaf was blanched at 25°C. All treatments were performed in triplicate. The extracts were centrifuged at 4,000 rpm for 10 min. Absorbances at 663 nm and 645 nm were measured using a spectrophotometer (UVICON-930, Kontron Instruments, Zürich, Switzerland) to determine the contents of chlorophyll (Chl) *a* and Chl *b* according to previous reported method by Wellburn (1994) (Wellburn, 1994). In addition, we may use the measured chlorophyll content to estimate N_0 and then use Equation 1 to simulate the *ETR*–*I* curves of leaves to obtain α_e, β_e, and γ_e, respectively. The values of σ_{ik} can be estimated by $\alpha_e = \frac{\alpha\beta N_0 \sigma_{ik} \varphi}{S}$ (in this study, α is 0.5, β is 0.84, φ is 0.95, and S is 6×10^{-4} m^2), the values of σ'_{ik} can be estimated by Equation 7 when the values of σ_{ik}, β_e, and γ_e were determined. *ETR*–*I* curves were fitted with the Photosynthesis Model Simulation Software (PMSS) at http://photosynthetic.sinaapp.com/index.html, in both Chinese and English, using Simulated Annealing and the Metropolis Algorithm to extract key parameters (e.g., α_e, β_e, γ_e, σ_{ik}, σ'_{ik}, ETR_{max}, and I_{sat}).

Statistical analyses

All variables are expressed as mean values ± *SE* from five samples for each species. Data were analyzed with one-way analysis of variance (ANOVA), and then, the values of ETR_{max} and I_{sat} estimated by four models were compared using a paired-sample *t*-test at $p < 0.05$ (*p*-significance level) using the SPSS 24.0 statistical software (SPSS, Chicago, IL). In addition, to compare the advantages and disadvantages of the study models, we took the Akaike's information criterion (*AIC*), mean absolute error (MAE), and determination coefficient (R^2) as indicators to assess the fitting results of the three models. *AIC* was calculated by reference to Akaike's method (Akaike, 1974), which equals $2k+n\times\ln(SSR/n)$ (here, k is the number of parameters, n is the sample size, and *SSR* is the sum square of residuals) and R^2 was given directly by SPSS 24.0 after fitting the data.

Results

Light response curves of *ETR*

All plant species exhibited a characteristic rapid initial increase in *ETR* with rising *I*, followed by a saturation phase (Figure 1). Both C_3 crops (*A. hypogaea* and *G. hirsutum*) displayed a slight decline in *ETR* beyond the saturation *I*, indicating a dynamic downregulation of PSII or photoinhibition (Figures 1A, B). The observed values of I_{sat} were approximately 1,600 μmol photons m^{-2} $s^{-1}$and 1,820 μmol photons m^{-2} s^{-1} for *A. hypogaea* and *G. hirsutum*, respectively, with the corresponding ETR_{max} values as approximately 195.49 μmol electrons m^{-2} s^{-1} and 228.83 μmol electrons m^{-2} s^{-1} (Figures 1A, B; Table 2). In contrast, the two cultivars of the C_4 crop *S. bicolor* showed less notable reduction in *ETR* after *I* surpassed I_{sat} (Figures 1C, D). The observed values of ETR_{max} for KFJT-1 and KFJT-4 were approximately 133.84 μmol electrons m^{-2} s^{-1} and 170.15 μmol electrons m^{-2} s^{-1}, respectively, with the corresponding I_{sat} values approximately 1,600 μmol photons m^{-2} s^{-1} (Figures 1C, D; Table 3).

Compared to Models 1, 2, and 4, Model 3 largely failed to represent the observed *ETR*–*I* curves (Figure 1). Models 1, 2, and 4 demonstrated high goodness-of-fit, based on the coefficient of determination (R^2) and mean absolute error (MAE) (Tables 2, 3). Although Model 4 showed higher R^2 values than Models 1 and 2 (Tables 2, 3), it overestimated ETR_{max} and cannot return I_{sat}. Models 1 and 2 provided ETR_{max} and I_{sat} values closely aligned with observed data across all species, but Model 1 demonstrated the lowest *AIC*, indicating an optimal balance between predictive accuracy and model parsimony. Model 3 underestimated both ETR_{max} and I_{sat}, with significant differences between fitted and measured data across all crops ($p<0.05$) (Figure 1C; Tables 2, 3). Additionally, despite Model 3 being able to produce F_v/F_m values by fitting *ETR*–*I* curves, these values significantly deviated from the observed F_v/F_m across all crops.

Light response curves of Φ_{PSII}

The four models varied significantly in characterizing Φ_{PSII}–*I* curves (Figure 2; Tables 4, 5). The Φ_{PSII}–*I* curves, fitted using Models 1 (Equation 6), 2 (Equation 14), 3 (Equation 16), and 4 (Equation 18), exhibited a characteristic decrease in Φ_{PSII} with the increasing *I* for all crops (Figure 2). Among the models, Model 1 most accurately simulated the nonlinear relationship between Φ_{PSII} and *I*, obtaining the highest R^2 and the lowest MAE compared to Models 2 and 3, which exhibited notable deviation from observations, particularly for *A. hypogaea* and *G. hirsutum* (Figures 2A, B; Tables 4, 5). Despite being able to estimate F_v/F_m, Model 3 produced F_v/F_m values that were significantly different from the measured values. Additionally, Model 3 generated an I_{sat} value with an unknown or unclear meaning (Tables 4, 5). While Model 4 exhibited the highest fitting degree for *G. hirsutum* and *S. bicolor* KFJT-4, the fitted curves fluctuated in the low light intensity range (below 600 μmol photons m^{-2} s^{-1}) (Figure 2). Furthermore, Model 4 generated a significantly higher ETR_{max} than the measured value. Another key difference among the models is their ability to return the $\Phi_{PSIImax}$. Models 1 and 2 can return $\Phi_{PSIImax}$, while Models 3 and 4 cannot. Compared to Model 2, Model 1 returned $\Phi_{PSIImax}$ values closer to the observed values.

Light response curves of *NPQ*, N_k and σ'_{ik}

NPQ increased nonlinearly with *I* across all plant species, with distinct patterns observed between C_3 and C_4 plants (Figures 3A–D).

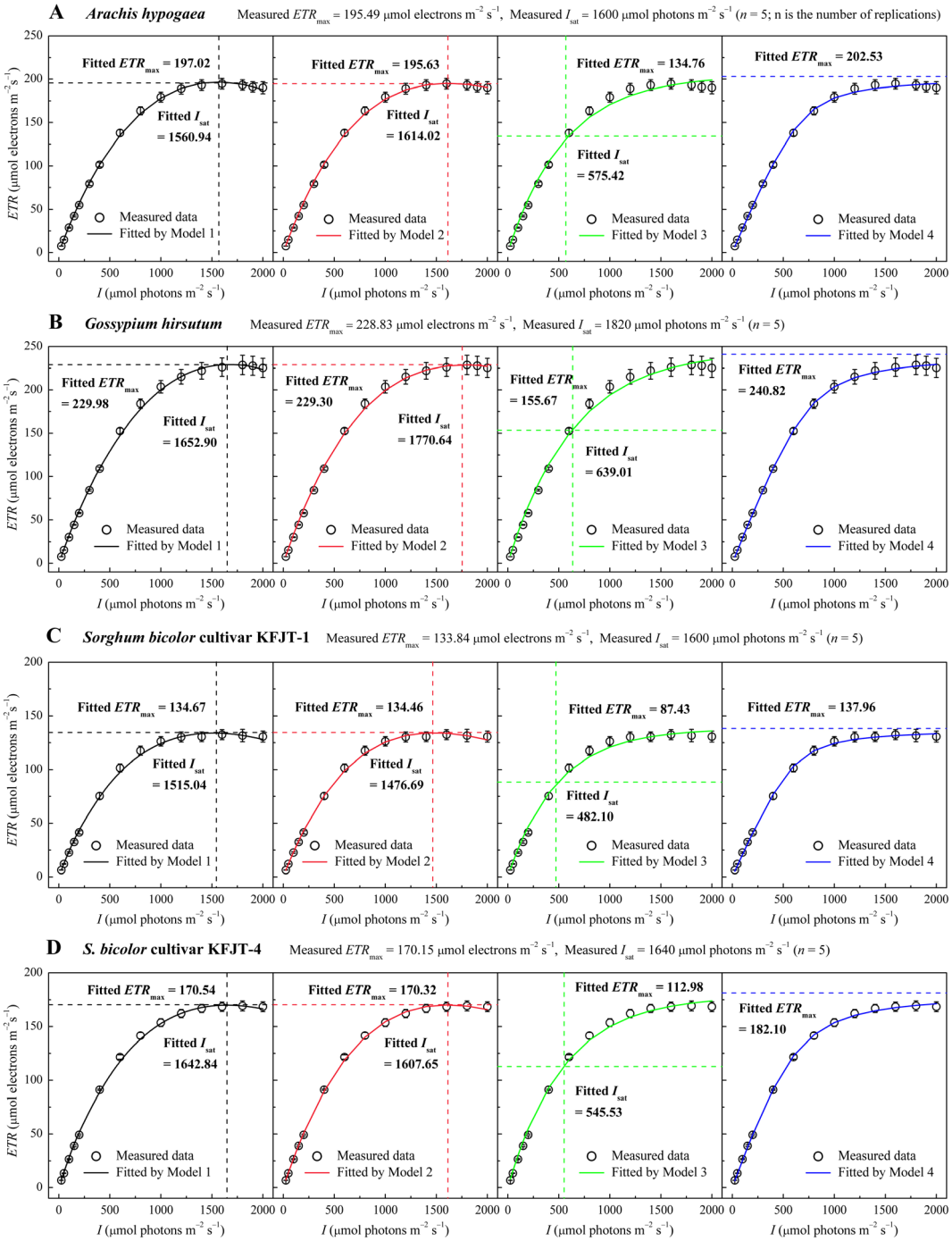

FIGURE 1
Light response curves of the electron transport rate (*ETR*–*I*) for various crops—*Arachis hypogaea* **(A)**, *Gossypium hirsutum* **(B)**, *Sorghum bicolor* cultivar KFJT-1 **(C)**, and *S. bicolor* cultivar KFJT-4 **(D)**. The curves were simulated by Models 1–4, respectively. Values were presented as means ± *SE* (n = 5). A horizontal dashed line represents the the fitted value of ETR_{max} from the model (μmol electrons m^{-2} s^{-1}), while a vertical dashed line represents the fitted value of I_{sat} from the model (μmol photons m^{-2} s^{-1}).

When I was below 600 μmol photons m^{-2} s^{-1}, the *NPQ* of *A. hypogaea* and *G. hirsutum* increased very slowly with the increasing *I*. When I was more than 600 μmol photons m^{-2} s^{-1}, *NPQ* increased rapidly (Figures 3A–D). In contrast, the *NPQ* of the two *S. bicolor* cultivars showed nearly linear increase when I was below 1,800 μmol photons m^{-2} s^{-1}. Under high I condition, the *NPQ* of *A. hypogaea* and *G. hirsutum* was significantly higher than that of the two *S. bicolor* cultivars. For example, at 1,800 μmol photons m^{-2} s^{-1}, the *NPQ* values of *A. hypogaea* and *G. hirsutum* were 1.54 and 1.35, respectively, whereas the *NPQ* values of the two *S. bicolor* cultivars

TABLE 2 Fitted (Equations 2, 13, 15, 19) and measured (Obs.) values of parameters defining *ETR–I* curves of *A. hypogaea* and *G. hirsutum*.

Parameters defining ETR–I curves	*A. hypogaea*					*G. hirsutum*				
	Model 1 (Equation 2)	Model 2 (Equation 13)	Model 3 (Equation 15)	Model 4 (Equation 19)	Obs.	Model 1 (Equation 2)	Model 2 (Equation 13)	Model 3 (Equation 15)	Model 4 (Equation 19)	Obs.
I_{sat}	1,560.94 ± 23.41^{a}	1,614.02 ± 46.45^{a}	575.42 ± 23.93^{b}	——	1,600.00 ± 63.24^{a}	1,652.90 ± 21.40^{b}	1,770.64 ± 62.61^{a}	639.01 ± 33.61^{c}	——	1,820.00 ± 20.00^{a}
ETR_{max}	197.02 ± 6.41^{a}	195.63 ± 6.11^{a}	134.76 ± 5.28^{b}	202.53 ± 6.21^{a}	195.49 ± 5.81^{a}	229.98 ± 10.76^{a}	229.30 ± 11.16^{a}	155.67 ± 8.99^{b}	240.82 ± 12.32^{a}	228.83 ± 11.00^{a}
$\Phi_{PSIImax}$	——	0.656 ± 0.005	——	——	——	——	0.750 ± 0.069	——	——	——
F_v/F_m	——	——	0.709 ± 0.026^{a}	——	0.726 ± 0.003^{a}	——	——	0.729 ± 0.033^{a}	——	0.722 ± 0.006^{a}
R^2	0.9991 ± 0.0002	0.9988 ± 0.0003	0.9929 ± 0.0008	0.9987 ± 0.0003	——	0.9989 ± 0.0001	0.9986 ± 0.0002	0.9945 ± 0.0001	0.9997 ± 0.0001	——
MAE	1.76 ± 0.30	2.00 ± 0.34	7.84 ± 2.59	2.09 ± 0.19	——	2.37 ± 0.10	2.67 ± 0.28	5.58 ± 0.24	1.12 ± 0.05	——
Number of parameters	3	4	4	3	——	3	4	4	3	——
AIC	19.08	23.05	32.28	21.19	——	21.82	25.52	32.20	13.30	——

The parameters are the saturation *I* (I_{sat}, μmol photons m^{-2} s^{-1}) and the maximum electron transport rate (ETR_{max}, μmol electrons m^{-2} s^{-1}). All values are the means ± *SE* (n = 5). Different letters denote statistically significant differences (p<0.05) between each row of fitted (Equations 2, 13, 15, 19) and measured (Obs.) values for each species. See Table 1 for definitions of abbreviations.

TABLE 3 Fitted (Equations 2, 13, 15, 19) and measured (Obs.) values of parameters defining *ETR–I* curves of two *S. bicolor* cultivars.

Parameters defining *ETR–I* curves	*S. bicolor* KFJT-1					*S. bicolor* KFJT-4				
	Model 1 (Equation 2)	Model 2 (Equation 13)	Model 3 (Equation 15)	Model 4 (Equation 19)	Obs.	Model 1 (Equation 2)	Model 2 (Equation 13)	Model 3 (Equation 15)	Model 4 (Equation 19)	Obs.
I_{sat}	1,515.04 ± 33.30^{a}	1,476.69 ± 33.56^{a}	482.10 ± 18.91^{b}	——	1,600.00 ± 63.24^{a}	1,642.84 ± 29.62^{a}	1607.65 ± 37.93^{a}	545.53 ± 20.00^{b}	——	1,640.00 ± 74.83^{a}
ETR_{max}	134.67 ± 5.05^{a}	134.46 ± 4.96^{a}	87.43 ± 3.45^{b}	137.96 ± 5.46^{a}	133.84 ± 5.52^{a}	170.54 ± 4.40^{b}	170.32 ± 4.33^{b}	112.98 ± 3.44^{c}	182.10 ± 4.97^{a}	170.15 ± 4.45^{b}
$\Phi_{PSIImax}$	——	0.672 ± 0.062	——	——	——	——	0.674 ± 0.028	——	——	——
F_v/F_m	——	——	0.675 ± 0.032^{a}	——	0.688 ± 0.004^{a}	——	——	0.672 ± 0.038^{a}	——	0.714 ± 0.001^{a}
R^2	0.9979 ± 0.0005	0.9976 ± 0.0008	0.9935 ± 0.0009	0.9985 ± 0.0003	——	0.9991 ± 0.0001	0.9991 ± 0.0002	0.9968 ± 0.0005	0.9994 ± 0.0002	——
MAE	1.90 ± 0.26	1.81 ± 0.23	3.47 ± 0.30	1.65 ± 0.19	——	1.61 ± 0.07	1.51 ± 0.09	3.20 ± 0.28	1.24 ± 0.17	——
Number of parameters	3	4	4	3	——	3	4	4	3	——
AIC	19.51	22.27	27.05	14.50	——	17.51	19.44	25.90	13.28	——

The parameters are the saturation *I* (I_{sat}, μmol photons m^{-2} s^{-1}) and the maximum electron transport rate (ETR_{max}, μmol electrons m^{-2} s^{-1}). All values are the means ± *SE* (n = 5). Different letters denote statistically significant differences (p<0.05) between each row of fitted (Equations 2, 13, 15, 19) and measured (Obs.) values for each species. See Table 1 for definitions of abbreviations.

10.3389/fpls.2025.1478346

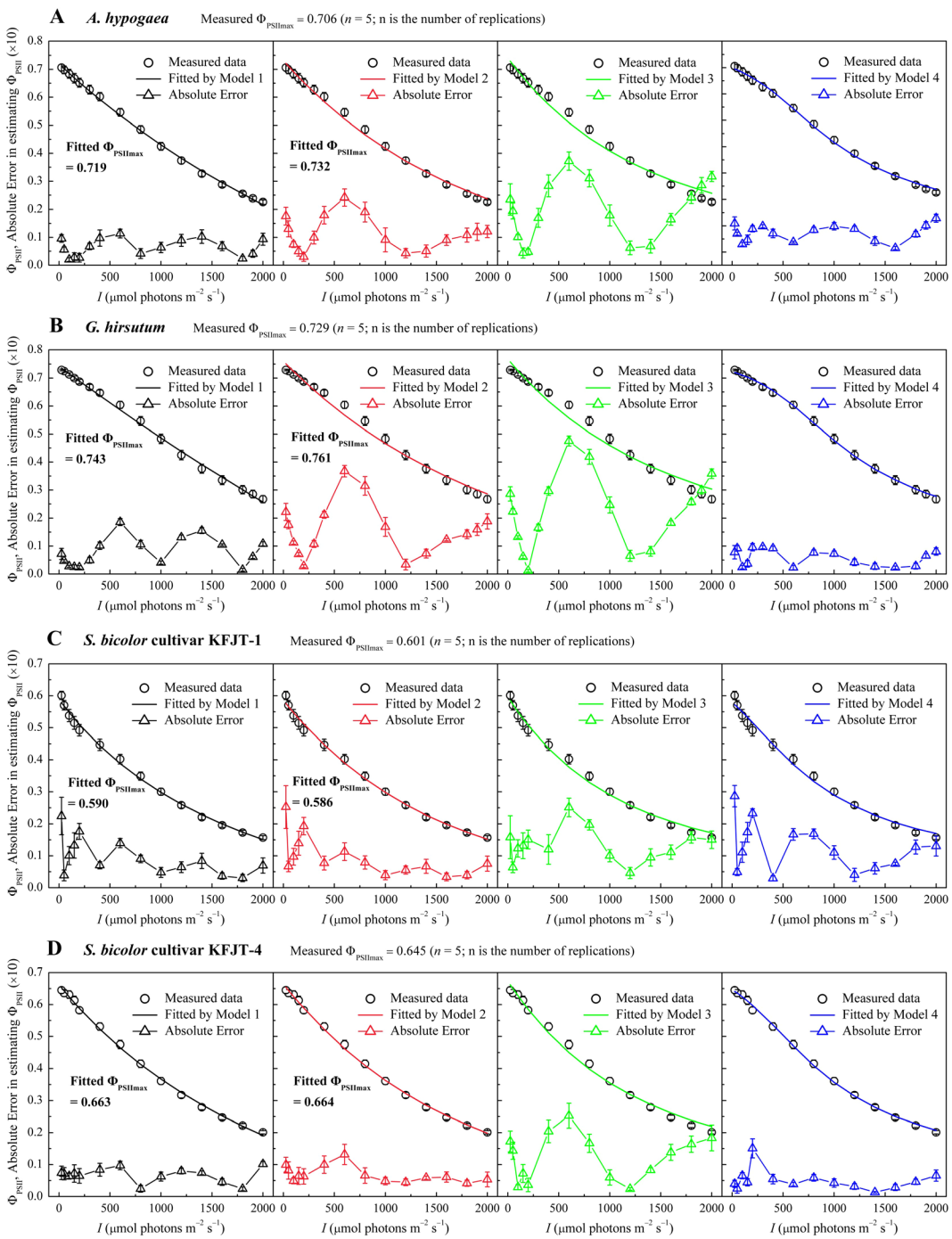

FIGURE 2
Light response curves of effective quantum efficiency (Φ_{PSII}–I) for various crops—*A. hypogaea* **(A)**, *G. hirsutum* **(B)**, *S. bicolor* cultivar KFJT-1 **(C)**, and *S. bicolor* cultivar KFJT-4 **(D)**. The curves were simulated by Model 1–4, respectively, and the fitted absolute error is shown. Values were presented as means ± *SE* (n = 5).

were only 0.77 and 0.81 (Figures 3A–D). N_k increased nonlinearly with the increasing I for all crops (Figure 3E–H), more rapidly in *S. bicolor* compared to that in *A. hypogaea* and *G. hirsutum*. At I = 1,800 μmol photons m^{-2} s^{-1}, the N_k values for *S. bicolor* cultivars KFJT-1 and KFJT-4 were 0.61 and 0.64, respectively, and *A. hypogaea* and *G. hirsutum* demonstrated lower N_k values (0.48 and 0.45, respectively).

During photosynthesis, light-harvesting pigment molecules absorb light energy and transition to different excited states. The ability of these molecules to absorb light energy is represented by their effective absorption cross-section (σ'_{ik}). As illustrated in Figures 3I–L, σ'_{ik} nonlinearly decreased with the increasing I for all crops, whose σ'_{ik}–I curves exhibited similar trends to their Φ_{PSII}–

TABLE 4 Fitted (Equations 6, 14, 16, 18) and measured (Obs.) values of parameters defining Φ_{PSII}–*I* curves of *A. hypogaea* and *G. hirsutum*..

Parameters defining Φ_{PSII}–*I* curves	*A. hypogaea*					*G. hirsutum*				
	Model 1 (Equation 6)	Model 2 (Equation 14)	Model 3 (Equation 16)	Model 4 (Equation 18)	Obs.	Model 1 (Equation 6)	Model 2 (Equation 14)	Model 3 (Equation 16)	Model 4 (Equation 18)	Obs.
$\Phi_{PSIImax}$	0.719 ± 0.016[a]	0.732 ± 0.017[a]	——	——	0.706 ± 0.012[a]	0.743 ± 0.004[b]	0.761 ± 0.006[a]	——	——	0.729 ± 0.003[b]
I_{sat}	——	——	747.37 ± 35.72	——	——	——	——	883.75 ± 55.85	——	——
F_v/F_m	——	——	0.742 ± 0.018[a]	——	0.726 ± 0.003[a]	——	——	0.769 ± 0.005[a]	——	0.722 ± 0.006[b]
ETR_{max}	——	——	——	212.73 ± 10.49	——	——	——	——	235.55 ± 6.96	——
R^2	0.9981 ± 0.0003	0.9939 ± 0.0017	0.9836 ± 0.0026	0.9913 ± 0.0060	——	0.9969 ± 0.0003	0.9877 ± 0.0026	0.9763 ± 0.0028	0.9985 ± 0.0002	——
MAE	0.0064 ± 0.0008	0.0112 ± 0.0015	0.0192 ± 0.0016	0.0074 ± 0.0007	——	0.0078 ± 0.0005	0.0156 ± 0.0012	0.0223 ± 0.0008	0.0060 ± 0.0005	——
Number of parameters	3	2	2	5	——	3	2	2	5	——
AIC	−36.60	−31.07	−26.06	−25.67	——	−34.79	−28.10	−24.72	−38.52	——

The parameters are the maximum effective quantum efficiency of PSII ($\Phi_{PSIImax}$), the saturation I (I_{sat}, μmol photons m^{-2} s^{-1}), the maximum quantum efficiency of PSII (F_v/F_m), and the maximum electron transport rate (ETR_{max}, μmol electrons m^{-2} s^{-1}). All values are the means ± *SE* (n = 5). Different letters denote statistically significant differences (p< 0.05) between each row of fitted (Equations 6, 14, 16, 18) and measured (Obs.) values for each light environment. See Table 1 for definitions of abbreviations.

TABLE 5 Fitted (Equations 6, 14, 16, 18) and measured (Obs.) values of parameters defining Φ_{PSII}–*I* curves of two *S. bicolor* cultivars.

Parameters defining Φ_{PSII}–*I* curves	*S. bicolor* KFJT-1					*S. bicolor* KFJT-4				
	Model 1 (Equation 6)	Model 2 (Equation 14)	Model 3 (Equation 16)	Model 4 (Equation 18)	Obs.	Model 1 (Equation 6)	Model 2 (Equation 14)	Model 3 (Equation 16)	Model 4 (Equation 18)	Obs.
$\Phi_{PSIImax}$	0.590 ± 0.018[a]	0.586 ± 0.019[a]	——	——	0.601 ± 0.013[a]	0.663 ± 0.011[a]	0.664 ± 0.013[a]	——	——	0.645 ± 0.010[b]
I_{sat}	——	——	597.87 ± 24.17	——	——	——	——	687.56 ± 23.40	——	——
F_v/F_m	——	——	0.598 ± 0.019[b]	——	0.688 ± 0.004[a]	——	——	0.675 ± 0.013[b]	——	0.714 ± 0.001[a]
ETR_{max}	——	——	——	144.55 ± 7.06	——	——	——	——	177.29 ± 7.90	——
R^2	0.9932 ± 0.0023	0.9926 ± 0.0025	0.9885 ± 0.0023	0.9894 ± 0.0031	——	0.9978 ± 0.0004	0.9973 ± 0.0004	0.9915 ± 0.0019	0.9983 ± 0.0005	——
MAE	0.0093 ± 0.0009	0.0095 ± 0.0009	0.0133 ± 0.0009	0.0126 ± 0.0014	——	0.0067 ± 0.0009	0.0069 ± 0.0008	0.0123 ± 0.0020	0.0050 ± 0.0009	——
Number of parameters	3	2	2	5	——	3	2	2	5	——
AIC	−33.12	−34.68	−32.26	−26.86	——	−36.22	−38.53	−32.73	−35.12	——

The parameters are the maximum effective quantum efficiency of PSII ($\Phi_{PSIImax}$), the saturation *I* (I_{sat}, μmol photons m^{-2} s^{-1}), the maximum quantum efficiency of PSII (F_v/F_m), and the maximum electron transport rate (ETR_{max}, μmol electrons m^{-2} s^{-1}). All values are the means ± *SE* (n = 5). Different letters denote statistically significant differences (p< 0.05) between each row of fitted (Equations 6, 14, 16, 18) and measured (Obs.) values for each light environment. See Table 1 for definitions of abbreviations.

10.3389/fpls.2025.1478346

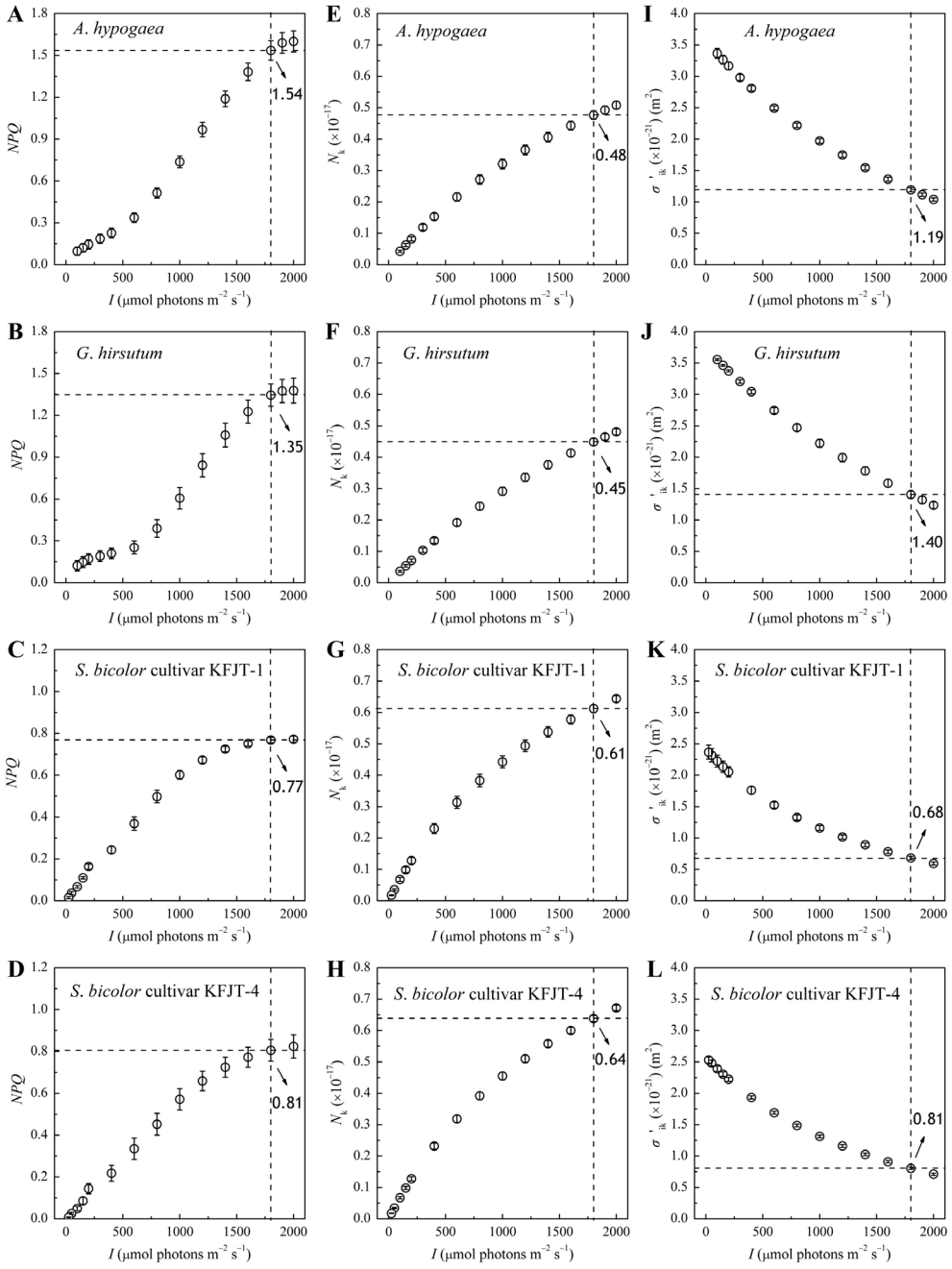

FIGURE 3
Non-photochemical quenching (*NPQ*), total light-harvesting pigment molecules in excited state (N_k), and effective light energy absorption cross-section (σ'_{ik}, m^2) for *A. hypogaea* **(A, E, I)**, *G. hirsutum* **(B, F, J)**, *S. bicolor* cultivar KFJT-1 **(C, G, K)**, and *S. bicolor* cultivar KFJT-4 **(D, H, K)**. Values were presented as means ± *SE* (n = 5). The intersection of the black horizontal and vertical dashed lines in each graph represents their measured value at I = 1,800 μmol photons m^{-2} s^{-1}.

I curves (Figure 2), indicating a strong correlation between light absorption and photosynthetic efficiency. Within the tested range of I, *A. hypogaea* and *G. hirsutum* exhibited significantly higher σ'_{ik} values compared to the two cultivars of *S. bicolor*. When I was 1,800 μmol m^{-2} s^{-1}, the σ'_{ik} of *A. hypogaea* and *G. hirsutum* were 1.19 × 10^{-21} m^2 and 1.40 × 10^{-21} m^2, respectively (Figures 3I, J), and the σ'_{ik} values of *S. bicolor* cultivars KFJT-1 and KFJT-4 were 0.68 × 10^{-21} m^2 and 0.81 × 10^{-21} m^2 (Figures 3K, L). σ_{ik} showed similar inter-specific difference as that of σ'_{ik}. The σ_{ik} values estimated by Model 1 (Equation 1) for *A. hypogaea* and *G. hirsutum* were (3.60 ± 0.10) ×

10^{-21} m^2 and (3.74 ± 0.23) × 10^{-21} m^2, respectively. The σ_{ik} values of *S. bicolor* cultivars KFJT-1 and KFJT-4 were (2.42 ± 0.12) × 10^{-21} m^2 and (2.58 ± 0.54) × 10^{-21} m^2, respectively.

Discussion

Empirical models and biological integration

Classic empirical models typically rely on mathematical analyses of measured data to establish quantitative functions, often lacking explicit incorporation of biological processes. Through the intercomparison among the four models and observations, this study demonstrates that Model 1 (Ye model) can accurately and simultaneously simulate *ETR*–*I* and Φ_{PSII}–*I* curves. Model 1 demonstrated its consistent robustness and accuracy for the studied crops in (1) reproducing the *ETR*–*I* and Φ_{PSII}–*I* curves and (2) returning key quantitative traits defining the light response functions.

By employing an explicit and transparent analytical framework with consistent definitions, Ye model incorporates the fundamental processes of light energy absorption, conversion, and transfer to the reaction centers of PSII via photosynthetic pigments. These processes include light harvesting, exciton resonance transfer, quantum level transitions, and de-excitation (Ye et al., 2013a, 2013b; Shevela et al., 2023). Equation 5 incorporated the quantitative relationship between Φ_{PSII} and the intrinsic characteristics of light-harvesting pigment molecules (i.e., N_0, σ_{ik}, τ, φ, k_P, k_D, g_i, g_k, ξ_1, ξ_2, and ξ_3. Our results highlight that the consistent decrease in Φ_{PSII} and σ'_{ik} with the increasing *I* (Figures 2, 3I–L), a finding consistent with previous studies (Suggett et al., 2004, 2007; Ye et al., 2013a).

Validation of model predictions

The observed decrease in σ'_{ik} with increasing *I* (Figures 3I–L) support previous studies (Suggett et al., 2004, 2007; Ye et al., 2013a). For instance, Suggett et al. (2004) reported the increase in effective absorption cross-sections for PSII of *Emiliania huxleyi* with the decrease in *I* in the plant growth environment. These results demonstrated that plants could adjust their light absorption properties to optimize photosynthetic efficiency and minimize photodamage under the changing light environment.

Moreover, the values of ETR_{max} and I_{sat} fitted by Ye model (Equation 2) were in close agreement with the observed data (Figure 1; Tables 2, 3), supporting previous reports (Ye et al., 2013a, 2013b; Robakowski et al., 2018). In contrast, Model 3 underestimated ETR_{max} and the corresponding I_{sat} (Figure 1; Tables 2, 3). While Model 4 has been widely used to estimate ETR_{max} and is a sub-model of FvCB model (Farquhar et al., 1980; von Caemmerer, 2000; Long and Bernacchi, 2003; Sharkey et al., 2007; Miao et al., 2009; Yin et al., 2009; Gu et al., 2010; Bernacchi et al., 2013; von Caemmerer, 2013; Park et al., 2016; Cai et al., 2018; Yin et al., 2021), it overestimated ETR_{max} and cannot return the corresponding I_{sat} (Figure 1; Tables 2, 3). These results support the previous studies reporting the limitations of these empirical models in accurately characterizing *ETR*–*I* curves (Smyth et al., 2004; Silsbe and Kromkamp, 2012; Buckley and Diaz-Espejo, 2015; Yang et al., 2024). Meanwhile, Ye model (Equation 6) can also accurately characterize the Φ_{PSII}–*I* curves (Figure 2; Tables 4, 5). The negative exponential function (Model 2) overestimated $\Phi_{PSIImax}$ (Figure 2; Tables 4). The exponential function (Model 3) and the NRH model (Model 4) cannot return $\Phi_{PSIImax}$ (Tables 4, 5).

Photosynthetic differences between C_3 and C_4 plants

Our study also highlights distinct photosynthetic responses between C_3 and C_4 plants. For instance, the Φ_{PSII} in *A. hypogaea* and *G. hirsutum* was significantly higher than that in two cultivars of *S. bicolor*, suggesting that C_3 plants may possess a greater capacity for light energy utilization compared to C_4 plants. The results demonstrate that Ye model (Model 1) can be used to estimate the absorption cross-section of pigment molecules for both C_3 and C_4 plants, supporting previous studies on other photosynthetic organisms (e.g., algae and cyanobacteria) (Yang et al., 2023; Ye et al., 2024). Ley and Mauzerall (1982) (Ley and Mauzerall, 1982) reported that the absolute absorption cross-section for oxygen production for chlorophyll in *Chlorella vulgaris* at 596 nm *in vivo* was 2.9×10^{-21} m^2, which was independent of total cell chlorophyll content. In this study, σ_{ik} estimated by Ye model (Equation 1) for *A. hypogaea*, *G. hirsutum*, *S. bicolor* KFJT-1, and *S. bicolor* KFJT-4 were 3.60 × 10^{-21} m^2, 3.74 × 10^{-21} m^2, 2.42 × 10^{-21} m^2 and 2.58 × 10^{-21} m^2, respectively.

C_3 and C_4 plants represent distinct evolutionary adaptations to different environmental conditions. The differences in their photosynthetic machinery and carbon fixation mechanisms lead to distinct responses in parameters such as Φ_{PSII}, *ETR*, and *NPQ* across light intensities (Stefanov et al., 2022). The different σ_{ik} values between C_3 and C_4 plants observed in this study reflect their differential adaptations to light environments. C_3 plants, which evolved in more moderate light environments, typically have a higher light absorption capacity (i.e., higher σ_{ik}). It allows them to efficiently capture light in potentially light-limited conditions. However, this higher absorption capacity also makes them more susceptible to photoinhibition at high light intensities, as observed in the *ETR*–*I* curves where *A. hypogaea* and *G. hirsutum* showed more notable decline in *ETR* beyond I_{sat} (Figure 1). In contrast, the C_4 plants (*S. bicolor*) in this study showed lower σ_{ik} values, contributing to their ability to maintain relatively constant *ETR* even when *I* surpasses I_{sat} (Figure 1). The carbon-concentrating mechanism allows C_4 plants to maintain high photosynthetic rates under high light conditions without the need for excessive light absorption, thereby reducing the risk of photodamage (Yang et al., 2024).

Model limitations and implications

While the Ye model provides a robust representation of light response mechanisms in PSII, it has limitations that warrant further research. The model assumes steady-state photosynthetic

conditions, which may not fully capture dynamic processes such as stomatal closure, changes in chloroplast morphology, or fluctuating light intensities. Additionally, factors such as nutrient availability, water stress, or temperature effects are not explicitly included in the current framework. These variables can significantly impact photosynthetic efficiency and could be integrated into future iterations of the model. This study validated the model on a limited set of crops (peanut, cotton, and sweet sorghum) under controlled conditions. Therefore, future studies should expand validation to a broader range of species (e.g., maize, rice, and wheat), and environmental contexts (e.g., fluctuating light, drought, and extreme temperatures) would strengthen the generalizability of model. Incorporating dynamic elements into the model to simulate transient responses to light fluctuations would be valuable. Furthermore, investigating the integration of abiotic stress factors into the model framework could improve predictions of photosynthetic efficiency under stress conditions such as drought or extreme heat.

The accurate assessment of key photosynthetic parameters, such as ETR_{max}, $\Phi_{PSIImax}$, I_{sat}, σ_{ik}, σ'_{ik}, N_k, and NPQ, positions the Ye model as a transformative tool for advancing photosynthetic research. These parameters are critical in understanding how plants respond to fluctuating light environments, optimize photochemical efficiency, and manage photoprotection. For instance, the ability of Ye model to quantify N_k and σ'_{ik} enables detailed exploration of how light-harvesting complexes dynamically adjust to varying light intensities. Similarly, the coupling of Φ_{PSII} and NPQ predictions provides insight into the balance between photochemical utilization and dissipation of excess light energy, a critical factor under high-stress conditions such as drought or extreme light fluctuations.

This capability has direct implications for plant breeding and crop management in the context of climate change. By leveraging the outputs of the model, researchers can identify genotypes with optimized light absorption and photoprotective traits for high light variability scenarios, such as those experienced in marginal or degraded agricultural lands. Moreover, the model can support breeding programs aimed at developing cultivars with enhanced yield stability by selecting for traits that mitigate photoinhibition or excessive NPQ under fluctuating light. Additionally, incorporating these parameter assessments into ecosystem and agricultural productivity models can improve predictions of carbon assimilation and crop yield under diverse environmental conditions.

To the best of our knowledge, this is the first study reporting a robust model (Equations 2, 6) that can simultaneously and accurately simulate ETR–I and Φ_{PSII}–I curves and returning values of key physical and biochemical parameters of photosynthetic pigments (i.e., intrinsic absorption cross-section and the effective absorption cross-section of light-harvesting pigment molecules). The findings could also help quantify key light-harvesting properties associated with photoacclimation (Fiebig et al., 2023), photoprotection (Niyogi and Truong, 2013), dynamic downregulation of PSII (Ralph and Gademann, 2005), and/or photoinhibition (Govindjee, 2002) in response to environmental change. This study is useful for (1) plant experimentalists quantifying intra- and/or inter-specific variation in Φ_{PSII}–I responses and (2) modelers working on better model representation of photosynthetic processes under dynamic light environment.

Data availability statement

The original contributions presented in the study are included in the article/supplementary material. Further inquiries can be directed to the corresponding authors.

Author contributions

X-LY: Conceptualization, Data curation, Formal analysis, Investigation, Methodology, Writing – original draft, Writing – review & editing. TA: Data curation, Formal analysis, Investigation, Writing – review & editing. Z-W-YY: Formal analysis, Software, Writing – review & editing. H-JK: Data curation, Formal analysis, Methodology, Writing – review & editing. PR: Methodology, Software, Writing – review & editing. F-BW: Data curation, Formal analysis, Software, Writing – review & editing. Z-PY: Conceptualization, Funding acquisition, Methodology, Software, Supervision, Writing – original draft, Writing – review & editing. S-XZ: Methodology, Writing – original draft, Writing – review & editing.

Funding

The author(s) declare that financial support was received for the research, authorship, and/or publication of this article. This work was supported by the National Natural Science Foundation of China (grant numbers 31960054, 41961005, and 31860045) and the Program for Construction of the Advantage Science and Technology Innovation Group of Jiangxi Province (grant number 20142BCB24010).

Conflict of interest

The authors declare that the research was conducted in the absence of any commercial or financial relationships that could be construed as a potential conflict of interest.

Publisher's note

References

Akaike, H. (1974). A new look at the statistical model identification. *IEEE T. Automat. Contr.* 19, 716–723. doi: 10.1109/TAC.1974.1100705

Baker, N. R. (2008). Chlorophyll fluorescence: a probe of photosynthesis *in vivo*. *Annu. Rev. Plant Biol.* 59, 89–113. doi: 10.1146/annurev.arplant.59.032607.092759

Bernacchi, C. J., Bagley, J. E., Serbin, S. P., Ruiz-Vera, U. M., Rosenthal, D. M., and Vanloocke, A. (2013). Modelling C_3 photosynthesis from the chloroplast to the ecosystem. *Plant Cell Environ.* 36, 1641–1657. doi: 10.1111/pce.2013.36.issue-9

Buckley, T. N., and Diaz-Espejo, A. (2015). Reporting estimates of maximum potential electron transport rate. *New Phytol.* 205, 14–17. doi: 10.1111/nph.13018

Buckley, T. N., and Farquhar, G. D. (2004). A new analytical model for whole-leaf potential electron transport rate. *Plant Cell Environ.* 27, 1487–1502. doi: 10.1111/j.1365-3040.2004.01232.x

Cai, C., Li, G., Yang, H., Yang, J., Liu, H., Struik, P. C., et al. (2018). Do all leaf photosynthesis parameters of rice acclimate to elevated CO_2, elevated temperature, and their combination, in FACE environments? *Global Change Biol.* 24, 1685–1707. doi: 10.1111/gcb.13961

Córdoba, J., Molina-Cano, J. L., Martínez-Carrasco, R., Morcuende, R., and Pérez, P. (2016). Functional and transcriptional characterization of a barley mutant with impaired photosynthesis. *Plant Sci.* 244, 19–30. doi: 10.1016/j.plantsci.2015.12.006

Ehleringer, J. J. O. (1981). Leaf absorptances of Mohave and Sonoran desert plants. *Oecologia* 49, 366–370. doi: 10.1007/BF00347600

Evans, J. R. (2009). Potential errors in electron transport rates calculated from chlorophyll fluorescence as revealed by a multilayer leaf model. *Plant Cell Physiol.* 50, 698–706. doi: 10.1093/pcp/pcp041

Farquhar, G. D., von Caemmerer, S., and Berry, J. A. (1980). A biochemical model of photosynthetic CO_2 assimilation in leaves of C_3 species. *Planta* 149, 78–90. doi: 10.1007/BF00386231

Fiebig, O. C., Harris, D., Wang, D., Hoffmann, M. P., and Schlau-Cohen, G. S. (2023). Ultrafast dynamics of photosynthetic light harvesting: atrategies for acclimation across organisms. *Ann. Rev. Phys. Chem.* 74, 493–520. doi: 10.1146/annurev-physchem-083122-111318

Genty, B., Briantais, J.-M., and Baker, N. R. (1989). The relationship between the quantum yield of photosynthetic electron transport and quenching of chlorophyll fluorescence. *BBA-Gen. Subj.* 990, 87–92. doi: 10.1016/S0304-4165(89)80016-9

Govindjee, (2002). A role for a light-harvesting antenna complex of photosystem II in photoprotection. *Plant Cell* 14, 1663–1668. doi: 10.1105/tpc.140810

Gu, L. H., Pallardy, S. G., Law, B. E., and Wullschleger, S. D. (2010). Reliable estimation of biochemical parameters from C_3 leaf photosynthesis-intercellular carbon dioxide response curves. *Plant Cell Environ.* 33, 1852–1874. doi: 10.1111/j.1365-3040.2010.02192.x

Krall, J. P., and Edwards, G. E. (1992). Relationship between photosystem II activity and CO_2 fixation in leaves. *Physiol. Plantarum* 86, 180–187. doi: 10.1111/j.1399-3054.1992.tb01328.x

Ley, A. C., and Mauzerall, D. C. (1982). Absolute absorption cross-sections for photosystem II and the minimum quantum requirement for photosynthesis in *Chlorella vulgaris*. *BBA-Bioenergetics* 680, 95–106. doi: 10.1016/0005-2728(82)90320-6

Liu, F., Song, Q., Zhao, J., Mao, L., Bu, H., Hu, Y., et al. (2021). Canopy occupation volume as an indicator of canopy photosynthetic capacity. *New Phytol.* 232, 941–956. doi: 10.1111/nph.17611

Long, S. P., and Bernacchi, C. J. (2003). Gas exchange measurements, what can they tell us about the underlying limitations to photosynthesis? Procedures and sources of error. *J. Exp. Bot.* 54, 2393–2401. doi: 10.1093/jxb/erg262

Maxwell, K., and Johnson, G. N. (2000). Chlorophyll fluorescence—a practical guide. *J. Exp. Bot.* 51, 659–668. doi: 10.1093/jexbot/51.345.659

Miao, Z., Xu, M., Lathrop, R. G. Jr., and Wang, Y. (2009). Comparison of the A–C_c curve fitting methods in determining maximum ribulose 1,5-bisphosphate carboxylase/oxygenase carboxylation rate, potential light saturated electron transport rate and leaf dark respiration. *Plant Cell Environ.* 32, 109–122. doi: 10.1111/j.1365-3040.2008.01900.x

Moin, M., Bakshi, A., Saha, A., Udaya Kumar, M., Reddy, A. R., Rao, K. V., et al. (2016). Activation tagging in indica rice identifies ribosomal proteins as potential targets for manipulation of water-use efficiency and abiotic stress tolerance in plants. *Plant Cell Environ.* 39, 2440–2459. doi: 10.1111/pce.12796

Niyogi, K. K., and Truong, T. B. (2013). Evolution of flexible non-photochemical quenching mechanisms that regulate light harvesting in oxygenic photosynthesis. *Curr. Opin. Plant Biol.* 16, 307–314. doi: 10.1016/j.pbi.2013.03.011

Park, K. S., Kim, S. K., Cho, Y.-Y., Cha, M. K., Jung, D. H., and Son, J. E. (2016). A coupled model of photosynthesis and stomatal conductance for the ice plant (*Mesembryanthemum crystallinum* L.), a facultative CAM plant. *Hortic. Environ. Biote.* 57, 259–265. doi: 10.1007/s13580-016-0027-7

Pavlovič, A., Slováková, L. U., Pandolfi, C., and Mancuso, S. (2011). On the mechanism underlying photosynthetic limitation upon trigger hair irritation in the carnivorous plant Venus flytrap (*Dionaea muscipula* Ellis). *J. Exp. Bot.* 62, 1991–2000. doi: 10.1093/jxb/erq404

Ralph, P. J., and Gademann, R. (2005). Rapid light curves: a powerful tool assesses photosynthetic activity. *Aquat. Bot.* 82, 222–237. doi: 10.1016/j.aquabot.2005.02.006

Ritchie, R. J. (2008). Fitting light saturation curves measured using modulated fluorometry. *Photosynth. Res.* 96, 201–215. doi: 10.1007/s11120-008-9300-7

Ritchie, R. J., and Bunthawin, S. (2010). The use of pulse amplitude modulation (PAM) fluorometry to measure photosynthesis in a CAM orchid, *Dendrobium* spp. (D. cv. Viravuth Pink). *Int. J. Plant Sci.* 171, 575–585. doi: 10.1086/653131

Robakowski, P. (2005). Susceptibility to low-temperature photoinhibition in three conifers differing in successional status. *Tree Physiol.* 25, 1151–1160. doi: 10.1093/treephys/25.9.1151

Robakowski, P., Pers-Kamczyc, E., Ratajczak, E., Thomas, P. A., Ye, Z.-P., Rabska, M., et al. (2018). Photochemistry and antioxidative capacity of female and male *Taxus baccata* L. acclimated to different nutritional environments. *Front. Plant Sci.* 9. doi: 10.3389/fpls.2018.00742

Sharkey, T. D., Bernacchi, C. J., Fa Rquhar, G. D., and Singsaas, E. L. (2007). Fitting photosynthetic carbon dioxide response curves for C_3 leaves. *Plant Cell Environ.* 30, 1035–1040. doi: 10.1111/j.1365-3040.2007.01710.x

Shevela, D., Kern, J. F., Govindjee, G., and Messinger, J. (2023). Solar energy conversion by photosystem II: principles and structures. *Photosynth. Res.* 156, 279–307. doi: 10.1007/s11120-022-00991-y

Silsbe, G. M., and Kromkamp, J. C. (2012). Modeling the irradiance dependency of the quantum efficiency of photosynthesis. *Limnol. Oceanogr. - Meth.* 10, 645–652. doi: 10.4319/lom.2012.10.645

Smyth, T. J., Pemberton, K. L., Aiken, J., and Geider, R. J. (2004). A methodology to determine primary production and phytoplankton photosynthetic parameters from Fast Repetition Rate Fluorometry. *J. Plankton Res.* 26, 1337–1350. doi: 10.1093/plankt/fbh124

Song, Q., Wang, Y., Qu, M., Ort, D. R., and Zhu, X.-G. (2017). The impact of modifying photosystem antenna size on canopy photosynthetic efficiency—Development of a new canopy photosynthesis model scaling from metabolism to canopy level processes. *Plant Cell Environ.* 40, 2946–2957. doi: 10.1111/pce.13041

Stefanov, M. A., Rashkov, G. D., and Apostolova, E. L. (2022). Assessment of the photosynthetic apparatus functions by chlorophyll fluorescence and P700 absorbance in C_3 and C_4 plants under physiological conditions and under salt stress. *Int. J. Mol. Sci.* 23, 3768. doi: 10.3390/ijms23073768

Suggett, D. J., Le Floc'H, E., Harris, G. N., Leonardos, N., and Geider, R. J. (2007). Different strategies of photoacclimation by two strains of *Emiliania huxleyi* (Haptophyta). *J. Phycol.* 43, 1209–1222. doi: 10.1111/j.1529-8817.2007.00406.x

Suggett, D. J., MacIntyre, H. L., and Geider, R. J. (2004). Evaluation of biophysical and optical determinations of light absorption by photosystem II in phytoplankton. *Limnol. Oceanogr. - Meth.* 2, 316–332. doi: 10.4319/lom.2004.2.316

van der Tol, C., Berry, J. A., Campbell, P. K. E., and Rascher, U. (2014). Models of fluorescence and photosynthesis for interpreting measurements of solar-induced chlorophyll fluorescence. *J. Geophys. Res.-Biogeo.* 119, 2312–2327. doi: 10.1002/2014JG002713

van Kooten, O., and Snel, J. F. H. (1990). The use of chlorophyll fluorescence nomenclature in plant stress physiology. *Photosynth. Res.* 25, 147–150. doi: 10.1007/BF00033156

von Caemmerer, S. (2000). *Biochemical models of leaf photosynthesis* (Victoria, Australia: CSIRO Publishing).

von Caemmerer, S. (2013). Steady-state models of photosynthesis. *Plant Cell Environ.* 36, 1617–1630. doi: 10.1111/pce.12098

Wang, B., Zhuang, Z., Zhang, Z., Draye, X., Shuang, L.-S., Shehzad, T., et al. (2017). Advanced backcross QTL analysis of fiber strength and fineness in a cross between *Gossypium hirsutum* and *G. mustelinum*. *Front. Plant Sci.* 8. doi: 10.3389/fpls.2017.01848

Webb, W. L., Newton, M., and Starr, D. (1974). Carbon dioxide exchange of *Alnus rubra*. *Oecologia* 17, 281–291. doi: 10.1007/BF00345747

Wellburn, A. R. (1994). The spectral determination of chlorophylls a and b, as well as total carotenoids, using various solvents with spectrophotometers of different resolution. *J. Plant Physiol.* 144, 307–313. doi: 10.1016/S0176-1617(11)81192-2

Xiao, Y., Tholen, D., and Zhu, X.-G. (2016). The influence of leaf anatomy on the internal light environment and photosynthetic electron transport rate: exploration with a new leaf ray tracing model. *J. Exp. Bot.* 67, 6021–6035. doi: 10.1093/jxb/erw359

Yang, X. L., Dong, W., Liu, L. H., Bi, Y. H., Xu, W. Y., and Wang, X. (2023). Uncovering the differential growth of *Microcystis aeruginosa* cultivated under nitrate and ammonium from a pathophysiological perspective. *ACS ES&T Water* 3, 1161–1171. doi: 10.1021/acsestwater.2c00624

Yang, X.-L., Ma, X.-F., Ye, Z.-P., Yang, L.-S., Shi, J.-B., Wang, X., et al. (2024). Simulating short-term light responses of photosynthesis and water use efficiency in

sweet sorghum under varying temperature and CO_2 conditions. *Front. Plant Sci.* 15. doi: 10.3389/fpls.2024.1291630

Ye, Z.-P., An, T., Govindjee, G., Robakowski, P., Stirbet, A., Yang, X.-L., et al. (2024). Addressing the long-standing limitations of double exponential and non-rectangular hyperbolic models in quantifying light-response of electron transport rates in different photosynthetic organisms under various conditions. *Front. Plant Sci.* 15. doi: 10.3389/fpls.2024.1332875

Ye, Z. P., Robakowski, P., and Suggett, D. J. (2013a). A mechanistic model for the light response of photosynthetic electron transport rate based on light harvesting properties of photosynthetic pigment molecules. *Planta* 237, 837–847. doi: 10.1007/s00425-012-1790-z

Ye, Z. P., Suggett, J. D., Robakowski, P., and Kang, H. J. (2013b). A mechanistic model for the photosynthesis-light response based on the photosynthetic electron transport of photosystem II in C_3 and C_4 species. *New Phytol.* 199, 110–120. doi: 10.1111/nph.12242

Yin, X., Busch, F. A., Struik, P. C., and Sharkey, T. D. (2021). Evolution of a biochemical model of steady-state photosynthesis. *Plant Cell Environ.* 44, 2811–2837. doi: 10.1111/pce.14070

Yin, X., Struik, P. C., Romero, P., Harbinson, J., and Vos, J. (2009). Using combined measurements of gas exchange and chlorophyll fluorescence to estimate parameters of a biochemical C_3 photosynthesis model: a critical appraisal and a new integrated approach applied to leaves in a wheat (*Triticum aestivum*) canopy. *Plant Cell Environ.* 32, 448–464. doi: 10.1111/j.1365-3040.2009.01934.x